FINAL TECHNICAL REPORT

Project Title: Advanced Energy and Water Recovery Technology from Low Grade Waste Heat

Award Number: DE-EE0003477

Project Period: August 16, 2010 to August 15 2011

Principal Investigator: Dexin Wang, 847-768-0533, Dexin.wang@gastechnology.org

Recipient Organization: Gas Technology Institute, 1700 South Mount Prospect Road, Des Plaines, IL 60018

Partners: Oak Ridge National Laboratory,
University of Tennessee, Knoxville,
Domtar Inc.

Date of Report: October 15, 2011

Acknowledgement

This report is based upon work support by the U.S. Department of Energy's Industrial Technology Program under Award No. DE-EE0003477.

Disclaimer

Any findings, opinions, and conclusions or recommendations expressed in this report are those of the author(s) and do not necessarily reflect the views of the Department of Energy.

Table of Contents

List of Acronym

Acronym	Definition
TMC	Transport Membrane Condenser
STM	Species Transport Model
MMM	Multiphase Mixture Model

List of Figures

List of Tables

List of Appendices

1. Executive Summary

The project has developed a nanoporous membrane based water vapor separation technology that can be used for recovering energy and water from low-temperature industrial waste gas streams with high moisture contents. This kind of exhaust stream is widely present in many industrial processes including the forest products and paper industry, food industry, chemical industry, cement industry, metal industry, and petroleum industry. The technology can recover not only the sensible heat but also high-purity water along with its considerable latent heat. Waste heats from such streams are considered very difficult to recover by conventional technology because of poor heat transfer performance of heat-exchanger type equipment at low temperature and moisture-related corrosion issues. During the one-year Concept Definition stage of the project, the goal was to prove the concept and technology in the laboratory and identify any issues that need to be addressed in future development of this technology.

In this project, computational modeling and simulation have been conducted to investigate the performance of a nanoporous material based technology, transport membrane condenser (TMC), for waste heat and water recovery from low grade industrial flue gases. A series of theoretical and computational analyses have provided insight and support in advanced TMC design and experiments. Experimental study revealed condensation and convection through the porous membrane bundle was greatly improved over an impermeable tube bundle, because of the membrane capillary condensation mechanism and the continuous evacuation of the condensate film or droplets through the membrane pores. Convection Nusselt number in flue gas side for the porous membrane tube bundle is 50% to 80% higher than those for the impermeable stainless steel tube bundle. The condensation rates for the porous membrane tube bundle also increase 60% to 80%. Parametric study for the porous membrane tube bundle heat transfer performance was also done, which shows this heat transfer enhancement approach works well in a wide parameters range for typical flue gas conditions. Better understanding of condensing heat transfer mechanism for porous membrane heat transfer surfaces, shows higher condensation and heat transfer rates than non-permeable tubes, due to existence of the porous membrane walls. Laboratory testing has documented increased TMC performance with increased exhaust gas moisture content levels, which has exponentially increased potential markets for the product. The TMC technology can uniquely enhance waste heat recovery in tandem with water vapor recovery for many other industrial processes such as drying, wet and dry scrubber exhaust gases, dewatering, and water chilling. A new metallic substrate membrane tube development and molded TMC part fabrication method, provides an economical way to expand this technology for scaled up applications with less than 3 year payback expectation.

A detailed market study shows a broad application area for this advanced waste heat and water recovery technology. A commercialization partner has been lined up to expand this technology to this big market. This research work led to new findings on the TMC working mechanism to improve its performance, better scale up design approaches, and economical part fabrication methods. Field evaluation work needs to be done to verify the TMC real world performance, and get acceptance from the industry, and pave the way for our commercial partner to put it into a much larger waste heat and waste water recovery market. This project is addressing the priority areas specified for DOE Industrial Technologies Program's (ITP's): Energy Intensive Processes (EIP) Portfolio - Waste Heat Minimization and Recovery platform.

2. Introduction

US industrial waste heat losses account for over 10 quadrillion Btu each year, representing 30.8% of the total energy used in the U.S. industry; hence a top energy saving opportunity. The majority of waste heat is of low grade, with features of lower temperature and high moisture content, as well as corrosive gases in many instances. The water vapor latent heat is substantial compared with the sensible heat associated with these temperatures and the water vapor itself is valuable. This kind of exhaust stream is widely present in many industrial processes including the forest, paper, food, chemical, cement, metal, and petroleum industries. Waste heats from such streams are considered very difficult to recover by conventional technologies because of equipment low heat transfer performance at low temperature and moisture-related corrosion issues. The TMC technology aims to be used for a broader range of low grade waste heat streams with high moisture. The project team has investigated a corrosion-resistant nanoporous ceramic membrane with good heat conductivity, working on a capillary condensation separation mechanism, to extract water vapor and its latent heat from the waste heat streams (a schematic as shown in Figure 1).

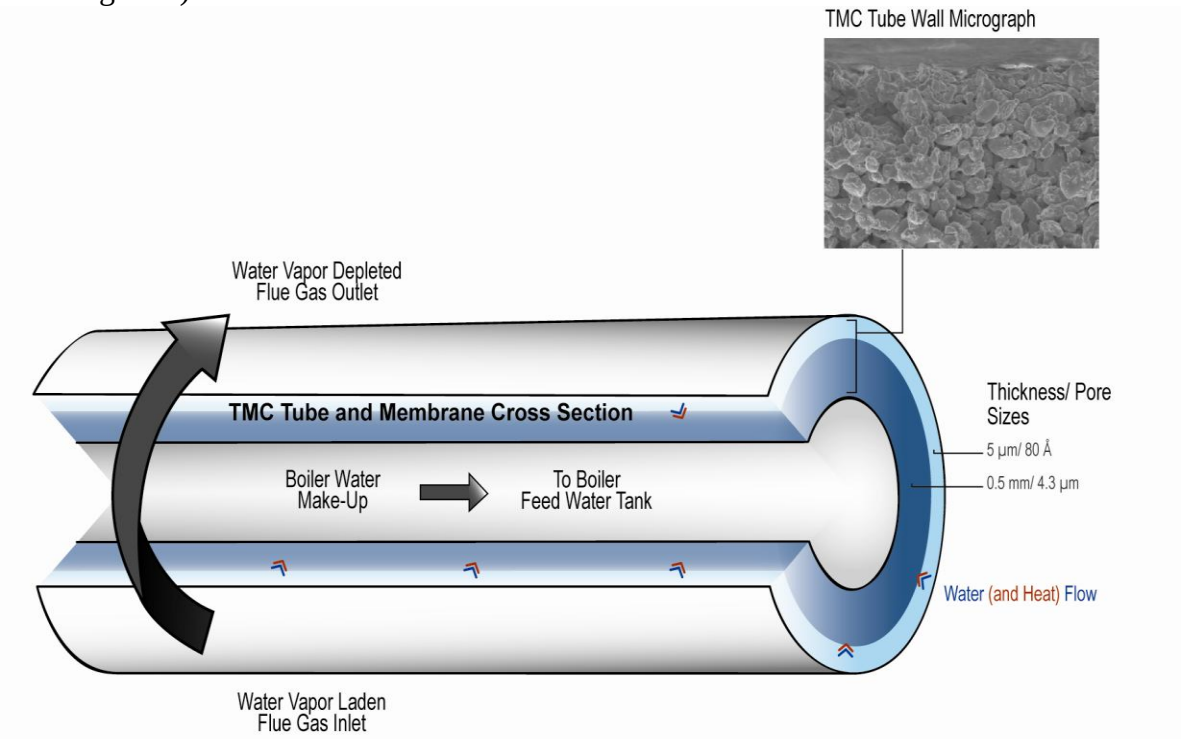

Figure 1: TMC concept, a single membrane tube with SS434 or SS316 as substrate is shown, and porous ceramic membrane coating (main component α alumina), each layer thickness/pore sizes are as shown

A very large low grade waste heat market exists across almost all US industries. Application of the TMC in these markets will significantly reduce energy consumption as well as a proportional decrease in greenhouse gas emissions while also recovering a large amount of water vapor in the form of usable water. We have collected low grade waste heat stream information from broad industrial applications in the past years, for applying the TMC technology. Three of them have been analyzed in details, which includes Pulp and Paper, Industrial Drying, and Alumina

Production. Their estimated annual energy savings are 252.5 TBtu with 23.8 billion gallons of water recovered, and 15.3 million tons of CO_2 and 6,173 tons of NO_x emissions can be avoided. For other applications, such as wet scrubbers which are widely used in refining industry, Portland cement industry, Iron and Steel industry, etc, their exhaust gas streams are of high moisture content and represent a good fit for the TMC technology. Flue gases from large industrial and utility boilers will be an even larger market. The project leading organization has a long history of successful commercialization of new technologies. It has licensed approximately 500 technologies that have generated estimated collective commercial revenues of more than $1 billion for the respective commercializers. We have also taken technologies to market through newly-formed ventures for that express purpose. For this particular technology, we are working with a major US boiler heat recovery equipment supplier, to bring it into the market place.

3. Background

A large portion of energy consumed today comes from hydrocarbon fuel combustion, and one of the major combustion products of this combustion is water vapor [1]. In natural gas fired industrial process units such as boilers, kilns, ovens, and furnaces, water vapor exits with the flue gases at a volume percentage up to 18%. Other industrial processes such as drying, wet scrubbers, dry scrubbers, dewatering, and water chilling, produce flue gases with 20-90% moisture content. Typically the water vapor along with its substantial latent heat is exhausted into the atmosphere [2] limiting thermal efficiency of these processes since no conventional heat recovery technique can effectively recover this low grade waste heat and water vapor. Exhaust gas temperature can certainly be reduced to its condensation temperature (dew point), but large heat transfer surfaces are required which typically are not economically favorable and corrosion due to condensation limits recovery of useful energy. If 40 to 60% of this water vapor and its latent heat could be recovered, thermal efficiency would increase by approximately 10% for most of these processes.

TMC working mechanism and research work

Gas separation membranes generally can be categorized as porous and non-porous. The separation of a mixture by non-porous membranes results from differences in the solubility and diffusivity of the various components in the membrane material [3]. Non-porous membranes usually display high separation ratios however their transport fluxes are relatively low [4, 5]. Porous membranes typically depend on some combination of molecular sieving, diffusivity, and surface effects to manage the segregation of gaseous species [6]. Porous membranes, depending on pore size can achieve higher transport fluxes than nonporous membranes but the separation ratio is usually much lower [4, 7, 8].

However, the vapor separation characteristics of porous membrane can be greatly improved under a condition wherein the vapor condenses within the membrane pore structure to such an extent that it completely blocks the pores and prevents the transport of the non-condensable gas components. Under such a condition, which is designated as the membrane capillary condensation mode, one observes dramatic increases in the membrane separation factor towards the condensable component (e.g., water vapor) [9, 10]. The condensed vapor transport through the membrane is thought to be governed by a pseudo-liquid phase transport; hence flux is much higher than expected from gas phase transport [11]. By working in this membrane capillary transport mode, porous membranes can achieve both high transport flux and high separation ratio.

Separating water vapor from a gas stream is a typical example of membrane separation involving a condensable component with phase change heat transfer. Relatively little investigation has been done for porous membranes working in the capillary condensation mode in the past. This is due to both the complicated nature of the capillary transport mode and historic perceptions that recovered water vapors are not commercially valuable. Only when increases in energy and water costs occurred did the importance of recovering water vapor and its latent heat found in various industrial exhausts make economic sense and the exploration of new techniques began to receive further attention. In addition, fresh water has become more valuable over the past decade and therefore recovered high quality water adds value for the technology development. Water

recovery from high moisture, elevated temperature waste streams is quite energy efficient since the water is already in a high energy state (vapor phase) and this energy can be eventually recovered along with the liquid water thereby increasing the overall system efficiency. It is the potential economic value of recovering such waste energy and water which justified investment in separating water vapor by membrane techniques.

Our experimental study found that a nanoporous ceramic membrane with a six nanometer mean pore size, when working in the Knudsen diffusion transport mode has low water vapor transport flux and poor separation characteristics, as expected. But when the gas stream is adequately cooled by heat transfer from the permeate side and the relative humidity of the flue gas increases, the capillary transport mode is produced in the porous membrane. Water vapor transport flux then increases by a factor of more than 5 from the value measured in the Knudsen diffusion mode (Figure 2) and the separation ratio is greatly improved by a factor of more than 100. Consequently, the onset of the membrane capillary condensation is a critical point for porous membrane vapor separation switching from a low performance mode to a high performance mode.

Figure 3 depicts the TMC concept for boiler applications with exhaust gas flowing on one side of a nanoporous ceramic membrane tube and cold boiler feed water flowing counter-current on the opposing side. Water vapor from the flue gas is transported through the membrane structure by first condensing inside the inner separation membrane layer (60Å to 80Å pore size), then moving through the intermediate layer (500Å pore size) and finally through the substrate (0.4 μm pore size). Other gas components in the flue gas are blocked from passing through the membrane by the condensed liquid. Condensed water along with its latent heat combines with the cold boiler feed water, helping to raise its temperature prior to entering the boiler feed water tank or deaerator. A small vacuum is maintained on the water side of the device to prevent backflow of water due to liquid pressure head and also to provide additional driving force for water to pass through the membrane.

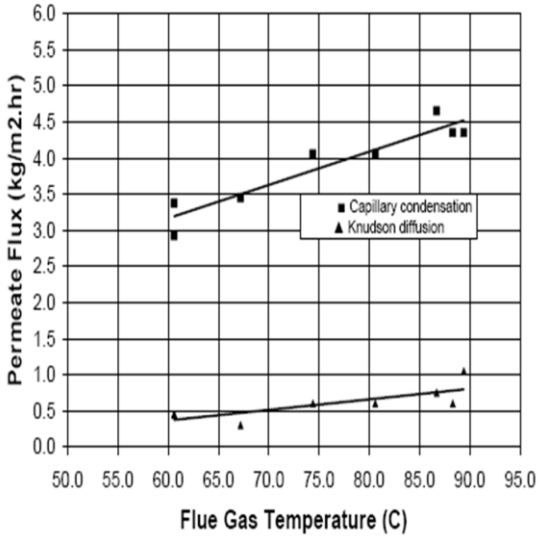

Figure 2: Membrane Transport Mode Effect

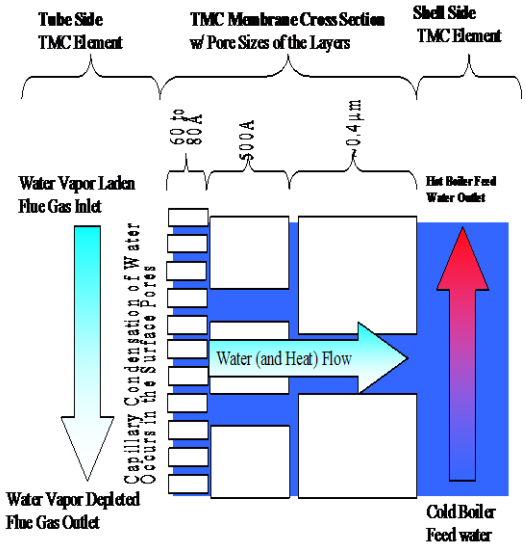

Figure 3: TMC Concept Schematic

For higher moisture content waste heat streams, the energy and water recovery potential is an advantage for using the TMC and we estimate 20 to 30% energy efficiency gain can be achieved in addition to the water recovery. Some challenges are present to achieve these goals.

- First, the membrane tube water transport flux must be increased to accommodate the high water transport rate expected for the high moisture content streams. This will be accomplished by improving the membrane porosity, pore size, and the pore structure such that the water transport flux can be increased.
- Second, the heat transfer through the membrane tube has to be adequate enough to transport all the latent heat released by the increased amount of water vapor condensation. Thermal conductivity of the membrane tube is a factor, but the condensing phenomenon on the gas side is more important because most of the heat transfer resistance is from the gas side.

Therefore, we investigated condensing heat transfer inside pore structures with non-condensable gases present in the stream by theoretical, modeling and experimental methods. A heat transfer enhancement method has been worked out to transfer significantly larger amount of heat for these high moisture content waste heat streams. After evaluating these two key factors, major corrosive gas components such as SO_2 were investigated to determine its impact on the TMC unit integrity and performance. Finally the selected membrane and heat transfer enhancement approaches were optimized for best TMC performance.

The project goals have been accomplished by performing the following Tasks:

1. Potential benefits assessment,

2. Modeling and theoretical studies,

3. Laboratory investigations,

4. Porous metallic membrane development for high transport flux,

5. TMC module design optimization,
6. Commercialization plan, and
7. Project management and reporting.

4. Results and Discussion

For this section, detailed results will be reported based on different methods we have used during this one year study.

4.1 Modeling and theoretical studies

Water vapor condensing phenomenon inside membrane pores is different for two reasons from surface condensation when the membrane pore size is in nanometer scale. First, based on the pore capillary condensation mechanism—Kelvin equation, pore condensation can occur when the local stream relative humidity is well below 100%, depending on the pore size, so earlier and larger amounts of water condensation are possible at the same surface temperature condition compared with surface condensation. Second, as the membrane continues to evacuate the condensed water to the permeate side, there is no water accumulation on the condensing surface, which eliminates the additional heat transfer resistance caused by the condensed liquid film (or droplets) that typically covers a non-permeating condensing surface. Theoretical and modeling methods have been used to study the pore condensation phenomenon to see its heat transfer enhancement effect over conventional surface condensation. Condensing performance of both surface condensation and pore condensation also depends on the waste stream non-condensable gas concentration or the moisture content. This effect has been considered in this study to define their different performance at different moisture content ranges. Theoretical and CFD modeling methods are mainly used for the study, with experimental results used to validate model constants and assist the analysis.

Species Transport Model

The species transport model (STM) is essentially the single-phase based transport model developed preciously by us. The model is implemented in CFD software Fluent using a user defined function (UDF). As shown in Fig.4, this model treats the TMC wall as solid wall, i.e., it does not resolve the heat and mass transfer inside the porous media of the tube wall. The condensation-evaporation process is considered as two-step chemical reactions only on the outer surface of the TMC tube:

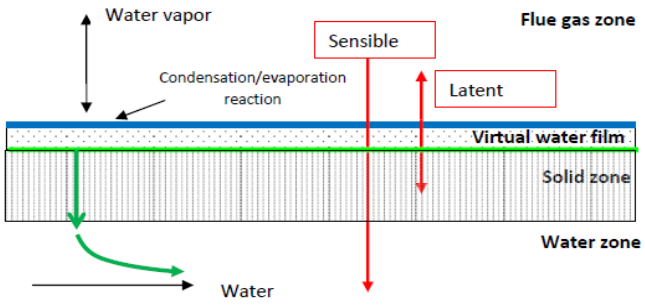

Figure 4: The species transport model.

$$H_2O(gas) \xleftrightarrow{Condensation/Evapration} H_2O(virtual\_mass) + heat \quad (1)$$

$$H_2O(virtual\_mass) \xleftrightarrow{Transfer} H_2O(liquid) \quad (2)$$

Using commonly used nomenclature, the governing equations for the species transport model are summarized as:

Continuity

$$\frac{\partial \rho}{\partial t} + \frac{\partial}{\partial x_i}(\rho u_i) = S_m \quad (3)$$

Momentum

$$\frac{\partial}{\partial t}(\rho u_i) + \frac{\partial}{\partial x_j}(\rho u_i u_j) = -\frac{\partial p}{\partial x_i} + \frac{\partial}{\partial x_j}\left[\mu\left(\frac{\partial u_i}{\partial x_j} + \frac{\partial u_j}{\partial x_i} - \delta_{ij}\frac{\partial u_l}{\partial x_l}\right)\right] + \frac{\partial}{\partial x_j}(-\overline{\rho u_i' u_j'}) + \rho g_i \quad (4)$$

Energy

$$\frac{\partial}{\partial t}(\rho E) + \frac{\partial}{\partial x_i}\left[u_i(\rho E + p)\right] = \frac{\partial}{\partial x_j}\left[\left(k + \frac{C_p \mu_t}{\mathrm{Pr}_t}\right)\frac{\partial T}{\partial x_j} + u_i(\tau_{ij})_{eff}\right] + S_h \quad (5)$$

Turbulence transport

$$\frac{\partial}{\partial t}(\rho k) + \frac{\partial}{\partial x_i}(\rho u_i k) = \frac{\partial}{\partial x_i}\left[(\alpha_k \mu_{eff}\frac{\partial k}{\partial x_i})\right] + \mu_t \tilde{S}^2 + G_b - \rho\varepsilon \quad (6)$$

$$\frac{\partial}{\partial t}(\rho\varepsilon) + \frac{\partial}{\partial x_i}(\rho u_i \varepsilon) = \frac{\partial}{\partial x_i}\left[(\alpha_\varepsilon \mu_{eff}\frac{\partial \varepsilon}{\partial x_i})\right] + C_{1\varepsilon}\frac{\varepsilon}{k}\mu_t S^2 - C_{2\varepsilon}\rho\frac{\varepsilon^2}{k} - R_\varepsilon \quad (7)$$

Species transport

$$\frac{\partial}{\partial t}(\rho Y_i) + \nabla\cdot(\rho \vec{\mathbf{u}} Y_i) = -\nabla\cdot\vec{J}_i + R_i + S_i \quad (8)$$

where, Y_i is the mass fraction of species i. Standard RNG k-ε turbulence model was used. **u** is the velocity vector, while u_i is velocity component in special direction i (i = 1,2,3).

To better represent the computational domain, a multi-block structured grid was generated. However, the previous developed UDF was found not working on this new grid with floating temperatures on the tube outer surfaces. Considering the fact that the species transport model assumes thermal equilibrium on the tube outer surfaces, we have used constant saturation temperatures on the tube outer surfaces for all the calculations.

Multiphase Mixture Model

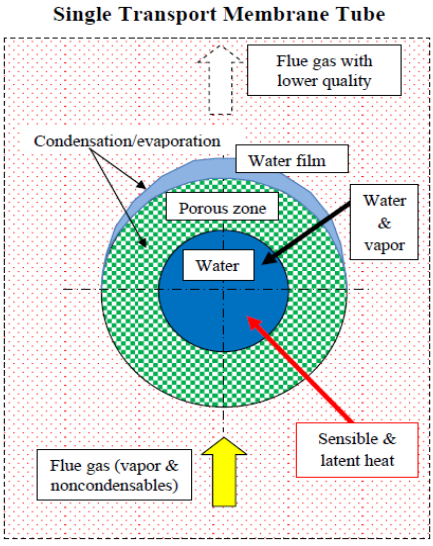

Figure 5: The multiphase mixture model.

The above species transport model is simple, but it considered the porous wall as a "black box". Particularly, it does not directly resolve the phase change processes inside and around the TMC tubes. To capture more physics encountered in the TMC tube bundle, we have developed a multiphase mixture model (MMM). The multiphase mixture model is a more realistic model, as it considers the condensation-evaporation processes not only inside the porous tube walls but also around the tube's outer surfaces. It treats the TMC tube wall as a porous medium. The condensation-evaporation phase change process is simulated with a mass transfer model. Figure 5 illustrated the basic concepts of phase change and heat transfer concepts in the multiphase mixture model.

In the multiphase mixture model, all the species in the flue gas are considered as phases. The turbulence model, RNG k-ε model, is the same as that used in the species transport model in equations (6) – (7). All the phases share the same continuity and momentum equations as a mixture "*m*":

Continuity and momentum equations of the mixture

$$\frac{\partial}{\partial t}(\rho_m) + \nabla \cdot (\rho_m \vec{v}_m) = 0 \quad (9)$$

$$\frac{\partial}{\partial t}(\rho_m \vec{v}_m) + \nabla \cdot (\rho_m \vec{v}_m \vec{v}_m) = -\nabla p + \nabla \cdot [\mu_m (\nabla \vec{v}_m + \nabla \vec{v}_m^T)] + \rho_m \vec{g} + \vec{F} + \nabla \cdot \left(\sum_{k=1}^{n} \alpha_k \rho_k \vec{v}_{dr,k} \vec{v}_{dr,k}\right) \quad (10)$$

In this project, we consider water vapor (H_2O) as the primary phase, all the other phases, including water liquid (H_2O-L), N_2, O_2 and CO_2, are considered as secondary phases. The volume fractions of secondary phases are computed by:

Volume fraction equation of secondary phases

$$\frac{\partial}{\partial t}\left(\alpha_p \rho_p\right) + \nabla \cdot \left(\alpha_p \rho_p \vec{v}_m\right) = -\nabla \cdot \left(\alpha_p \rho_p \vec{v}_{dr,p}\right) + \sum_{q=1}^{n} (\dot{m}_{qp} - \dot{m}_{pq}) \quad (11)$$

In addition, the multiphase mixture model will require a porous model for the TMC wall and a condensation-evaporation model for the phase change. These two models are summarized in the following:

Porous Media Model

- Source term in momentum equation

$$S_i = -\left(\sum_{j=1}^{3} D_{ij} \mu v_j + \sum_{j=1}^{3} C_{ij} \frac{1}{2} \rho |v| v_j\right) \quad (12)$$

- Energy equation

$$\frac{\partial}{\partial t}\left(\gamma \rho_f E_f + (1-\gamma)\rho_s E_s\right) + \nabla \cdot \left(\vec{v}\left(\rho_f E_f + p\right)\right) = \nabla \cdot \left[k_{eff} \nabla T - \left(\sum_i h_i J_i\right) + (\bar{\bar{\tau}} \cdot \vec{v})\right] + S_f^h \quad (13)$$

where, E_f is total fluid energy, E_s total solid medium energy, γ porosity of the medium, k_{eff} effective thermal conductivity of the medium, and S_f^h fluid enthalpy source term.

Condensation-Evaporation Model

- Phase-phase mass transfer (mechanistic model)

$$\text{If } T > T_{sat} \qquad \dot{m}_{l \to v} = coeff * \alpha_l \rho_l \frac{(T - T_{sat})}{T_{sat}} \quad (14)$$

$$\text{If } T < T_{sat} \qquad \dot{m}_{v \to l} = coeff * \alpha_v \rho_v \frac{(T - T_{sat})}{T_{sat}} \quad (15)$$

- *coeff* (condensation or evaporation frequency, *cf*)
  Theoretical expression for coeff or *cf* is based on flat surface:

$$coeff = \frac{6}{d}\beta\sqrt{\frac{M}{2\pi RT_{sat}}}L\left(\frac{\rho_l}{\rho_l-\rho_g}\right) \quad (16)$$

Equation (16) does not work for the tube surfaces. However, we can take an engineering approach to fine-tune its value based on available experimental data.

Numerical Computations

The governing equations of the models were solved by a control volume method, implemented in commercial CFD software. A high performance Linux cluster with parallel computing capability was used for all the numerical computations. Convergence was ensured by checking residual levels below a fixed value and the overall balances of energy and mass in the computational domain.

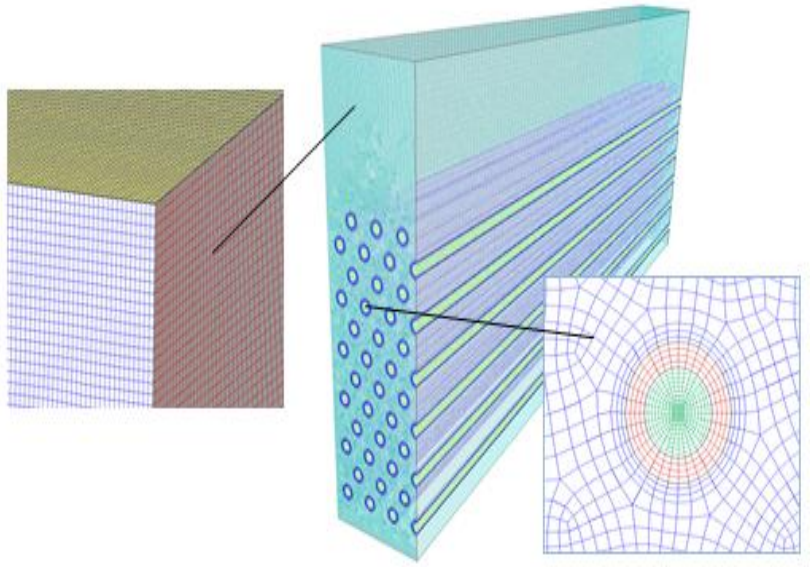

Figure 6: 3D Grid for 3D Simulation.

Figure 6 shows the 3D multi-block structured grid used in the numerical simulations. Most of the cells are of either hex or paved types. The total number of cells in the grid is 3.31 millions. Due to the symmetry of the geometry, only half of the tube bundle with 39 porous/solid tubes was modeled.

All equations were solved using numerical schemes of second-order accuracy (UPWIND), except for volume fractions, which were solved using schemes of third-order accuracy (QUICK).

Selected Simulation Results and Discussions

Model Validation and Comparison

Table 1 shows the comparison of the water exit temperature, flue gas exit temperature, and flue gas exit mass fraction obtained by experiments, species transport model (STM), and multiphase mixture model (MMM) for the baseline case. As can be seen from the Table, both STM and MMM agree with the experimental data fairly well. The MMM intends to be more accurate than STM, but requires that the condensation frequency be optimized against experimental data.

Table 1. Comparison between experimental and computational results.

	Exp.	STM	MMM*	STM Error (%)	MMM Error (%)
Flue gas exit temperature (F)	138.9	145.0	137.2	4.39%	-1.22%
Water exit temperature (F)	134.5	133.8	130.7	-0.52%	-2.8%
Vapor exit mass fraction (%)	10.31	9.51	10.96	-7.76%	6.30%

*Condensation frequency = 100, not optimized.

Using the experimental data, we have also conducted a comprehensive validation study of the species transport model (STM). Figure 7 shows the comparison between computational prediction and experimental measurement of condensation rates at different surface temperature. Figure 8 quantitatively characterizes the deviation of the computational results from the experimental data. As can be seen from the figures, within relatively high surface temperature (or low condensation rate) range, the computational results agree fairly well with experimental data. At low surface temperature, the STM over predicts the condensation rate. This also implicates that the STM could generate larger errors at lower surface temperature (or higher condensation rate).

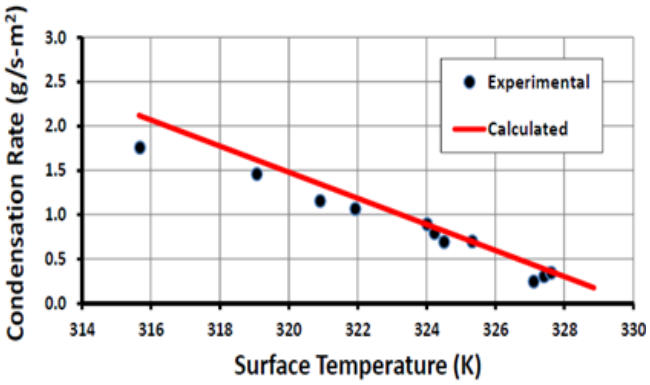

Figure 7: Comparison between computational and experimental data.

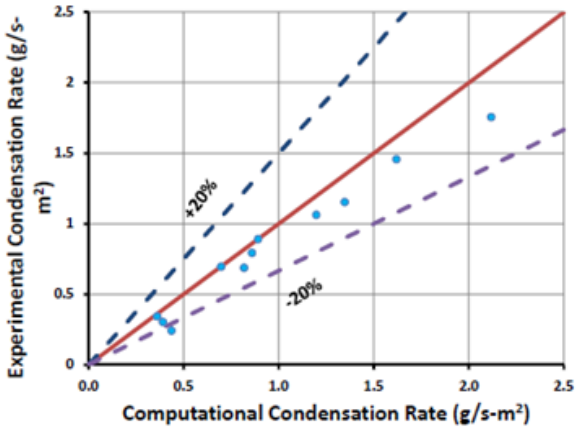

Figure 8: Deviation of computational results from experimental data.

During the course of the project, we have also performed a systematic optimization studies of condensation/evaporation frequencies in the MMM model using the available TMC experimental data.

<u>Comparison between STM and MMM</u>

We have performed preliminary comparative study of STM and MMM in tube bundle simulations. Figure 9 shows the typical temperature fields predicted by STM and MMM on the middle plane of a TMC tube bundle. Although in terms of average exit temperature, STM prediction agrees fairly well with MMM as shown in Table 1, a careful inspection of the temperature contours in Figure 9 shows the difference in local thermal fields predicted by the two models.

Figure 10 shows the velocity vectors on the middle plane of the TMC bundle under the same condition as Figure 9. In general, there are less "red" or lower velocity vectors in the MMM results. This is because some fluids are flowing into the tube in radial direction in the MMM simulation, resulting relatively lower total velocity magnitude around the TMC tube.

A close-up of the flow field round the tubes in the

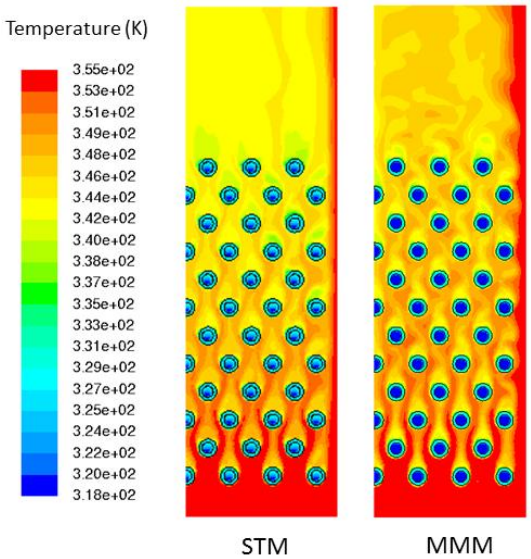

Figure 9: STM vs. MMM: Middle Plane Temperature (TMC, *cf*=10, Re_{Dh} = 2.6×10^4).

STM and MMM are also provided in Fig.10. As it can be seen from the Fig.10, the MMM predicted the velocity vectors inside the porous wall of TMC tubes. For the results by STM, there is no any velocity vector predicted in the TMC tube wall as no porous model was used.

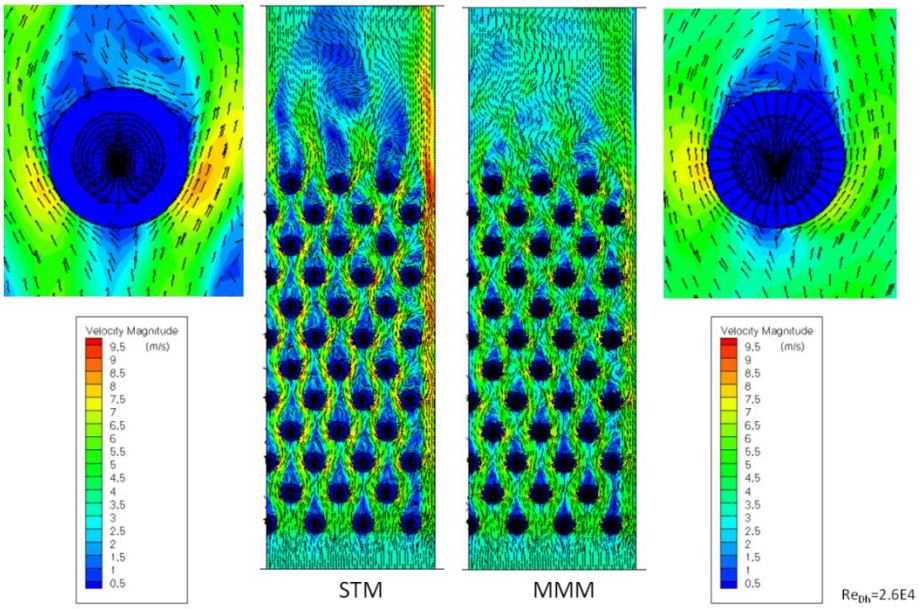

Figure 10: STM vs. MMM: Middle Plane Velocity Vectors (TMC, *cf*=10, $Re_{Dh} = 2.6\times10^4$)

The following provides a summary of the advantages and disadvantages of the species transport model (STM) and multiphase mixture model (MMM) based on our current study.

STM

- Advantages
  - Simple
  - Less CPU hours
  - Accuracy fairly good as compared to experimental data
- Disadvantages
  - Fluid flows and mass transfer in the porous wall not resolved
  - Liquid film on the outside wall of TMC tube not resolved

MMM

- Advantages
  - Higher fidelity
  - More physics: condensation & evaporation via mass transfer
  - Fluid flows mass transfer in the porous wall resolved
- Disadvantages
  - More CPU hours
  - Mass transfer model coefficients needed to be fine tuned
  - More input data: inertial & viscous resistance factors for porous media

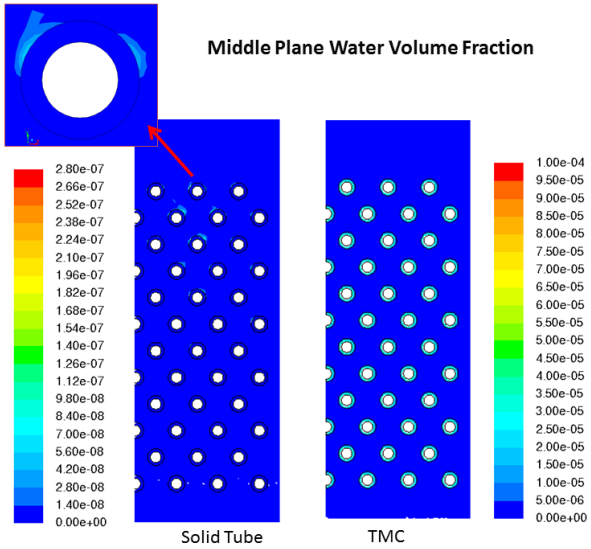

Figure 11: Solid tube vs. TMC porous tube: liquid water volume fraction (*cf* = 10).

Comparison between TMC Porous Tubes and Solid Tubes

We have performed a comparison of the performance of the TMC porous tubes and the regular sold wall tubes using MMM. Figure 11 shows the volume fraction of liquid water on the middle plane of the tube bundle. As can be seen, water film was formed on the outer surface of solid tube wall, while water contents appeared inside the TMC porous wall.

The water film formed on the outer surfaces of solid tubes is also shown in a 3D representation in Figure 12. It is obvious in the region close to cooling water inlet and near the flue gas exit, more liquid water are formed due to condensation.

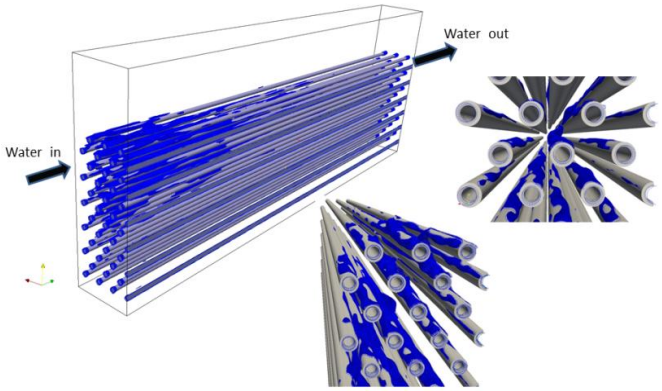

Figure 12: Water film on the solid wall tubes (*cf* = 10).

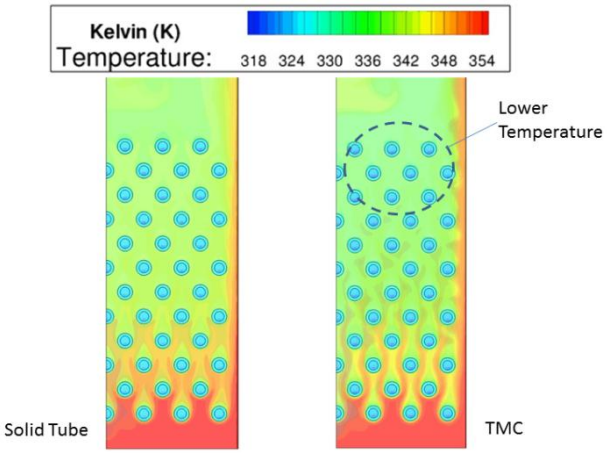

Figure 13: Solid tube vs. TMC porous tube: temperature contours on the middle plane (*cf* = 0.1).

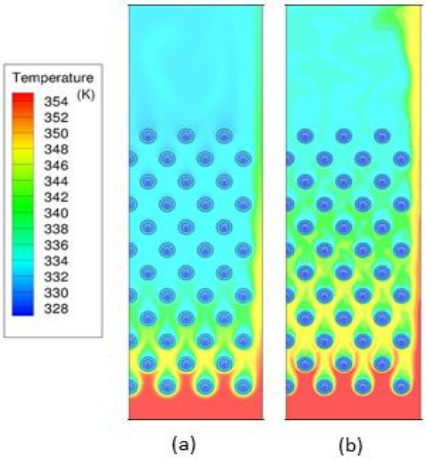

Figure 14: Temperature fields on the middle plane. (a) $Re_{Dh} = 1.0\times10^3$; (b) $Re_{Dh} = 3.6\times10^3$.

Figure 13 shows the comparison of typical temperature contours for solid wall tubes and TMC porous wall tubes on the middle plane of the bundle. For the case of TMC porous tubes, the temperature levels near the flue gas exit are lower as compared to the solid wall tube case. This indicates that TMC porous tubes can recover more waste heat than the solid tube – more heat has been depleted causing lower temperature. As condensation heat transfer occurs at the same time, this also implies that the TMC porous tubes will have higher condensation rate than the solid tubes under the same conditions.

<u>Effects of Reynolds Number and Temperature</u>

We have investigated the effects of flue gas inlet temperature and Reynolds number on the waste heat/water recovery performance of the TMC module. Figure 14 shows the typical temperature fields on the middle plane of the TMC module at two flue gas inlet Reynolds numbers. Here, Re_{Dh} is based on the hydraulic diameter and properties of the flue gas at the experimental module's channel inlet. As can be seen from the figure, the areas of lower temperature at lower flue gas Reynolds number is larger than that at higher flue gas Reynolds number.

Figure 15 shows the typical mass fraction fields of water vapor on the middle plane of the TMC module at two flue gas inlet Reynolds numbers. Similar to the temperature fields, the areas of lower vapor mass fraction at lower flue gas Reynolds number is larger than that at higher flue gas Reynolds number, particularly in the region close to the upper section of the tube bundle. This reflects the fact that at lower flue gas Reynolds number, more water vapor has been condensed into liquid water, resulting lower

vapor mass fraction levels. Figure 16 shows the vapor mass fraction on the symmetric plane of the tube bundle. As cooling water flows from left to right, the vapor mass fraction on the left is lower on the right at both Reynolds numbers.

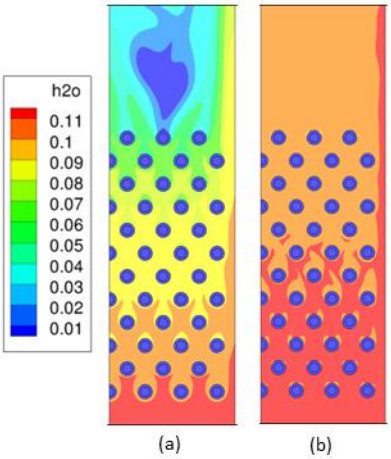

Figure 15: Mass fraction of water vapor on the middle plane. (a) $Re_{Dh} = 1.0\times10^3$; (b) $Re_{Dh} = 3.6\times10^3$.

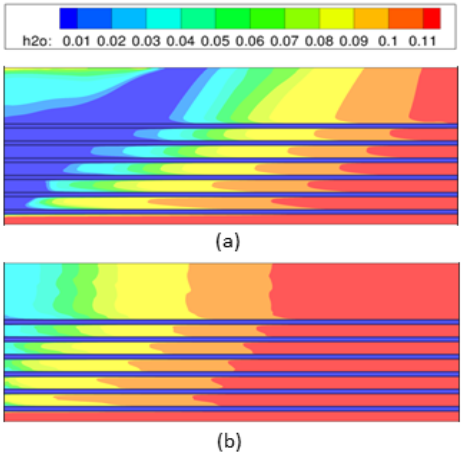

Figure 16: Mass fraction of water vapor on the symmetric plane (y-z). (a) $Re_{Dh} = 1.0\times10^3$; (b) $Re_{Dh} = 3.6\times10^3$.

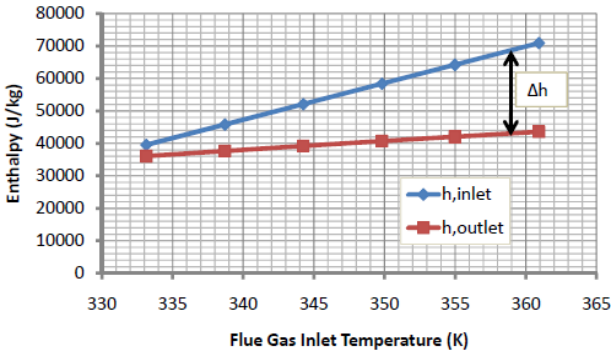

Figure 17: Enthalpy changes with flue gas inlet temperature.

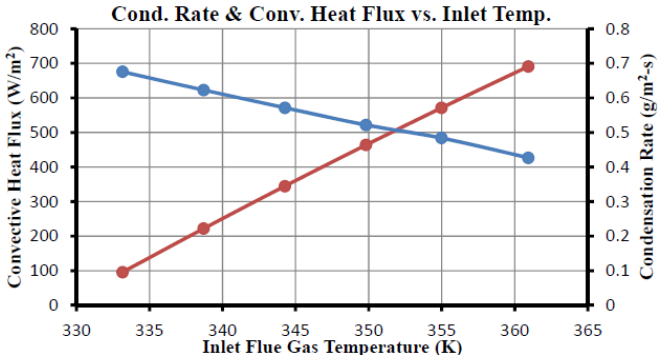

Figure 18: Convective heat fluxes and condensation rates at different flue gas inlet flue gas inlet temperature.

Figure 17 shows the flue gas enthalpy change, $\Delta h = h_{out} - h_{in}$, of the module with flue gas inlet temperature. The enthalpy change represents the waste heat recovered by the TMC. It can be seen from the figure that the waste heat recovered increases almost linearly with the increase of the flue gas inlet temperature.

Figure 18 shows the variations of convective heat fluxes and condensation rates within a range of flue gas inlet temperature. As shown in the figure, convective heat transfer will increases while condensation rate will decreases with the increase of flue gas inlet temperature. This behavior makes sense from heat transfer standpoint.

Figure 19 shows the effects of Reynolds number on the heat and mass depletions through the TMC module. Here the heat depletion is defined as the temperature change from flue gas inlet to outlet. The mass depletion is the water vapor mass fraction change from flue gas inlet to outlet. It seems the TMC module performs better, i.e. the heat and mass depletions are

higher, when the flue gas flows at lower Reynolds numbers. This make sense as well, as at lower Reynolds numbers, the flue gas has higher residence time in the module to undergo condensation process.

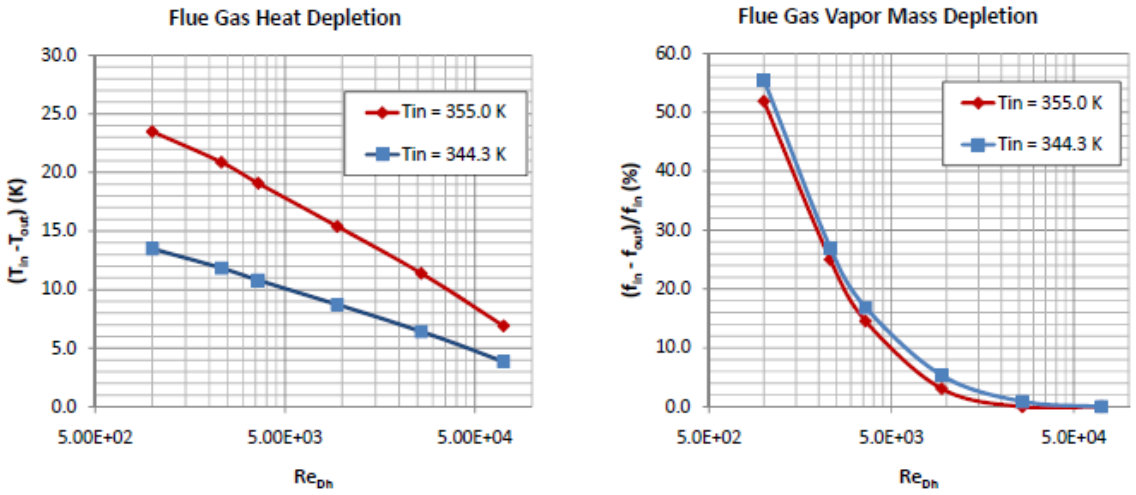

Figure 19: Heat and mass depletions at different Reynolds numbers.

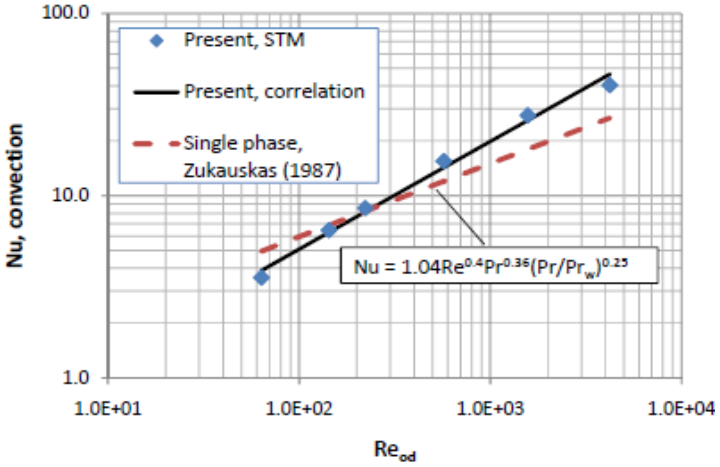

Figure 20: Convective Nusselt number vs. Reynolds number Re_{od}.

Figure 20 shows the convective Nusselt numbers at different Reynolds number Re_{od}, which is based on the outer diameter of the tube and the mean velocity in the minimum intertube space u_0. It should be noted that Re_{od} and Re_{Dh} are related. Also shown is the correlation from the classic work of Zukauskas (1987) for single-phase flow heat transfer over solid tube bundles. It seems that the flue gas's convective heat transfer (not the total heat transfer) over the TMC tube bundle is at the same order of single-phase fluid over solid tube bundle. The difference in the convective heat transfer for flue gas (with phase change) and single-phase fluids (without phase change) is reflected in the deviation of the curve's slopes shown in the figure.

Based on our numerical results, the following heat transfer correlation is developed within our investigated parameter ranges:

$$Nu = 0.37Re^{0.59}Pr^{0.36}(Pr/Pr_w)^{0.25} \quad (17)$$

where the same correction $(Pr/Pr_w)^{0.25}$ for single phase flow is used for the flue gas flow.

Local Distributions of Skin Friction and Heat Transfer

Numerical results have been analyzed in details to investigate the local distribution of skin friction coefficients and convective Nusselt number along the surfaces of the TMC tubes at different flue gas Reynolds numbers. The complex behaviors of the local skin fraction coefficient and convective Nusselt number reflect the complexity in turbulent flow patterns and phase-change processes near the walls of the tube bundles.

Figure 21 shows the local skin friction coefficients vs angle θ at two flue gas Reynolds numbers. Here, the θ is defined as the angle between flue gas flow direction and the radial direction of a point on the circular cross-section of the tube's outside wall, and is measured from the stagnation point ($\theta = 0^o$). As can be seen from Figs. 21 (a) and (b), the local distribution of the skin friction coefficient is rather complicated. Generally speaking, the first row's local skin friction coefficient is quite different from other rows. The highest values of skin friction coefficient occur when $\theta = 30 - 60^o$.

Figure 22 shows the corresponding local convective Nusselt number vs angle θ at two flue gas Reynolds numbers. Similar to local skin friction factor, the first row's convective Nusselt number behaves differently from most of the other rows. However, for most of the rows, the highest values of convective Nusselt number are located near the stagnation point.

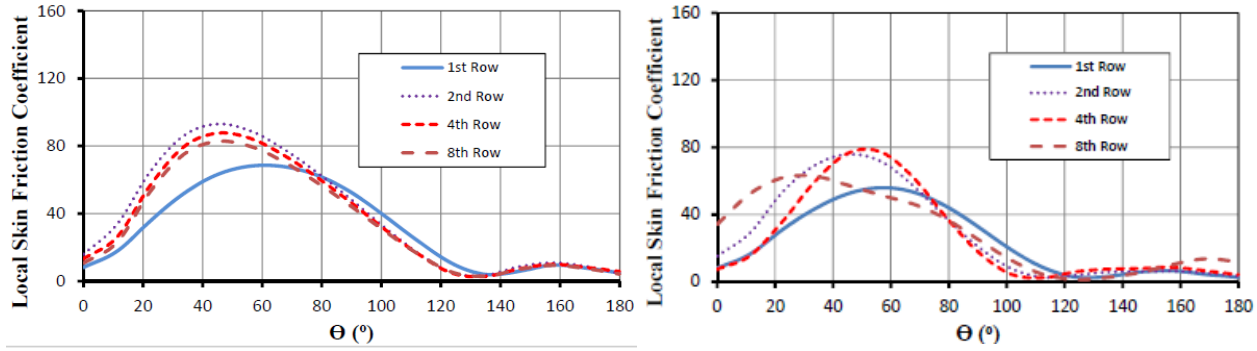

(a) (b)

Figure 21: Local skin friction coefficient vs. angle on the middle plane. (a) $Re_{Dh} = 1.0\times10^3$; (b) $Re_{Dh} = 3.6\times10^3$.

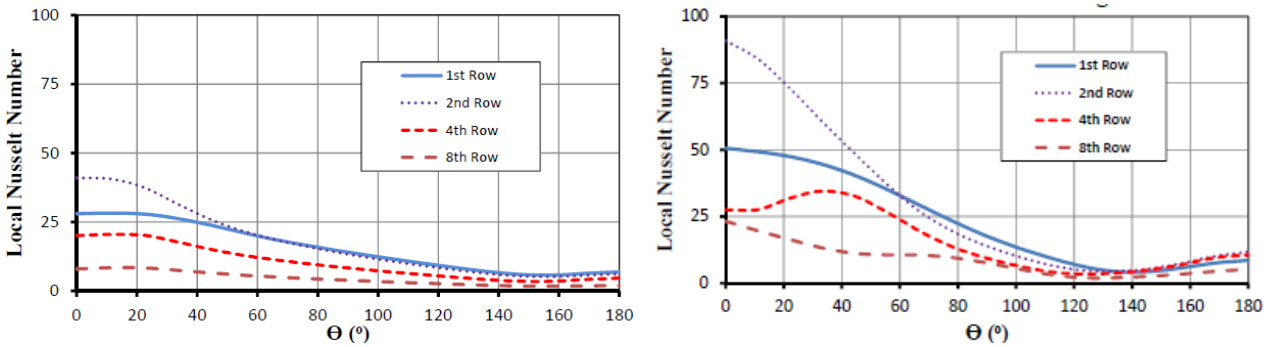

(a) (b)

Figure 22: Local convective Nusselt numbers vs. angle on the middle plane. (a) $Re_{Dh} = 1.0\times10^3$; (b) $Re_{Dh} = 3.6\times10^3$.

Figures 21 and 22 also show that both skin friction and convective heat transfer are lowest in the near-wake regions of the tubes.

Experimental data have been used to perform detailed validation study of the STM and MMM models as mentioned above.

4.2 Laboratory Experimental Investigation

Experimental study has been performed to study membrane pore condensation heat transfer enhancement effects. Tests have been done for a typical condensing heat exchanger material, for example, stainless steel tubes, as a baseline case for non-permeating condensing surface. Then a condensing heat exchanger made from a nanoporous membrane material was studied for its heat transfer performance, with pore size in nanometer ranges to achieve the capillary condensation effect. At the same test condition, the two condensing phenomenon was compared with each other to prove if pore condensation is superior to surface condensation. The greater porous membrane heat transfer performance offer an opportunity to use nanoporous membrane material to build condensing heat exchangers to recover both water vapor and its substantial amount of latent heat from low grade high moisture waste heat streams.

Nanoporous membrane tube heat transfer enhancement study

A nanoporous ceramic membrane tube bundle (or called TMC module) and an impermeable stainless steel tube bundle with the same characteristic dimensions were built to study pore condensation heat transfer enhancement effects. Both bundles have 78 tubes in 12 rows with a staggered arrangement. The longitudinal pitch S1 is 13.6 mm, the transverse pitch S2 is 8.8 mm, and the tube length L is 43.2 cm, for both bundles. All geometrical parameters for the porous membrane tube bundle and the impermeable stainless steel tube bundle are shown at Table 2. The impermeable tubes are made from 304 stainless steel.

Table 2. Dimensions of the impermeable tube bundle and porous membrane tube bundle

	Stainless steel tube	Porous membrane tube
Material	Stainless steel 304	Alumina (porosity 30%)
Outer diameter (d_o)	6.3 mm	5.5 mm
Inner diameter (d_i)	4.7 mm	3.5 mm
Wall thickness	0.8 mm	1 mm
Length (L)	43.2 cm	43.2 cm
Cross section for flue	43cm x 9cm	43cm x 9cm
Longitudinal pitch (S1)	13.6 mm	13.6 mm
Transverse pitch (S2)	8.8 mm	8.8 mm
Number of tubes (n)	78	78

Experiments have been carried out to compare the heat and mass transfer performance between the porous membrane tube bundle and the impermeable stainless steel tube bundle, with similar Reynolds numbers. Figure 23 is the schematic of the experimental apparatus.

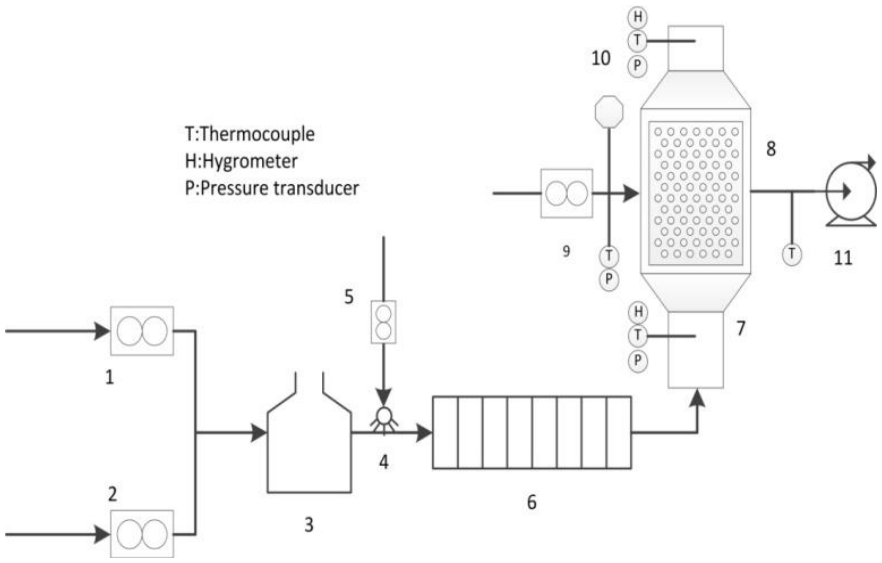

Figure 23: Schematic of experimental apparatus: 1 Natural gas flow meter; 2 Compressed air flow meter; 3 Natural gas combustor; 4 Water injection nozzle; 5 Water flow meter; 6 Flue gas cooling section; 7 Test duct; 8 Porous membrane tube bundle or stainless steel tube bundle; 9 Cooling water flow meter; 10 Vacuum generator; 11 Cooling water pump

The relationship of the convection Nusselt number in flue gas side versus Mean Temperature Difference （MTD） is shown in Fig. 24. The relationship of the mass transfer coefficient versus MTD is shown in Fig. 25, and mass transfer coefficients g_m represents condensation rates of both bundles as:

$$g_m = \frac{m_{cond}}{A} \tag{18}$$

Where A is the bundle surface area, and m_{cond} is the condensation rate. Figure 26 shows the relationship of overall Nusselt numbers versus MTD for both the porous membrane tube bundle and the impermeable stainless steel tube bundle.

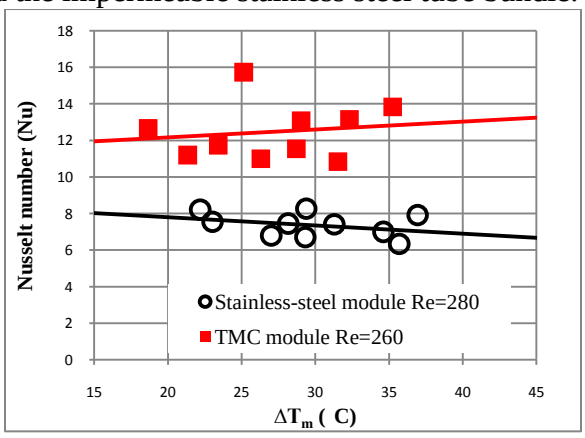

Figure 24: MTD effect on convection Nusselt number in flue gas side

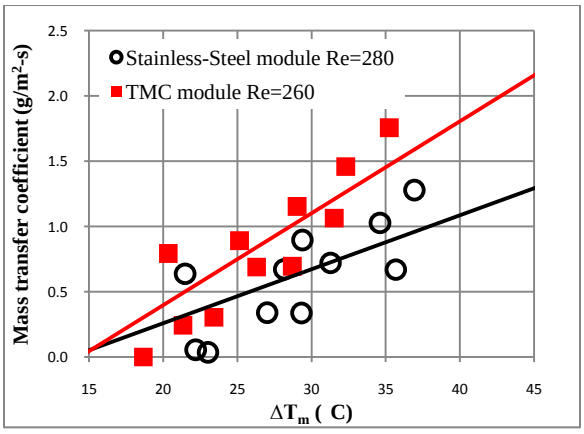

Figure 25: MTD effect on ondensation rate

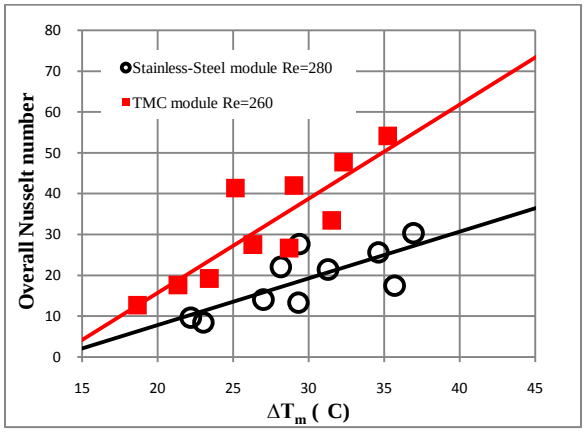

Figure 26: MTD effect on overall Nusselt number

The results confirm a more than 50% heat transfer enhancement for the porous membrane tubes bundle, compared with the impermeable tubes bundle.

Parametric study for TMC performance

Parametric study of the porous membrane tube bundle was conducted by varying flue gas side and cooling water side conditions. The results are shown in Figures 27-31. From Figure 27, there is an optimized ratio between the flue gas flow rate and membrane surface area, at certain cooling water conditions. As shown in Figures 30-31, when cooling water inlet temperature decreases, or water flow rate increases, water and heat recovery rates are boosted. Similarly, lower flue gas inlet temperature and higher flue gas inlet dew point increase moisture and heat recovery rates. The parametric study shows the TMC module works well in a wide parameters range for typical flue gas conditions.

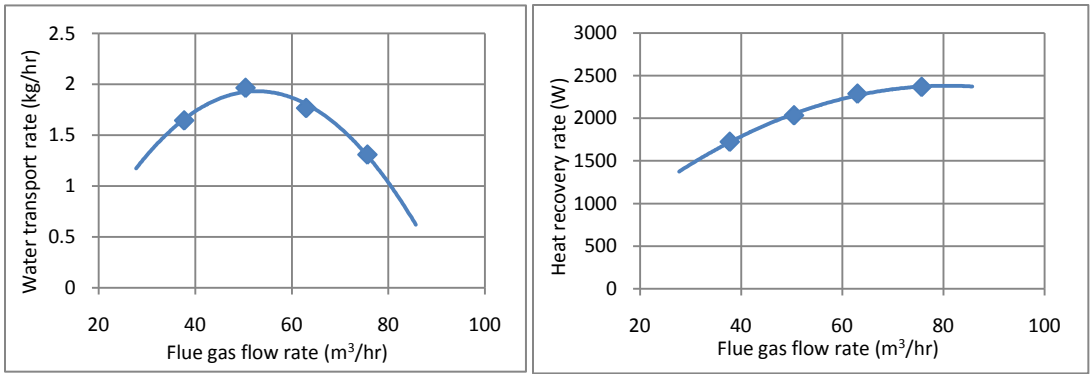

Figure 27: Flue gas flow rate effect on TMC performance (Flue inlet T@82°C; Flue inlet Td@56°C; Water flow rate@1.25kg/min; Water inlet T@25°C)

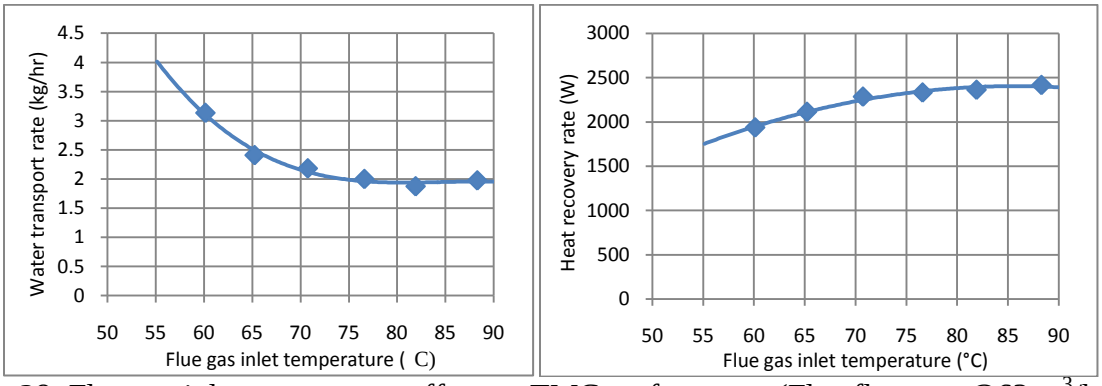

Figure 28: Flue gas inlet temperature effect on TMC performance (Flue flow rate@63 m^3/h; Flue inlet Td@56°C; Water flow rate@1.25kg/min; Water inlet T@25°C)

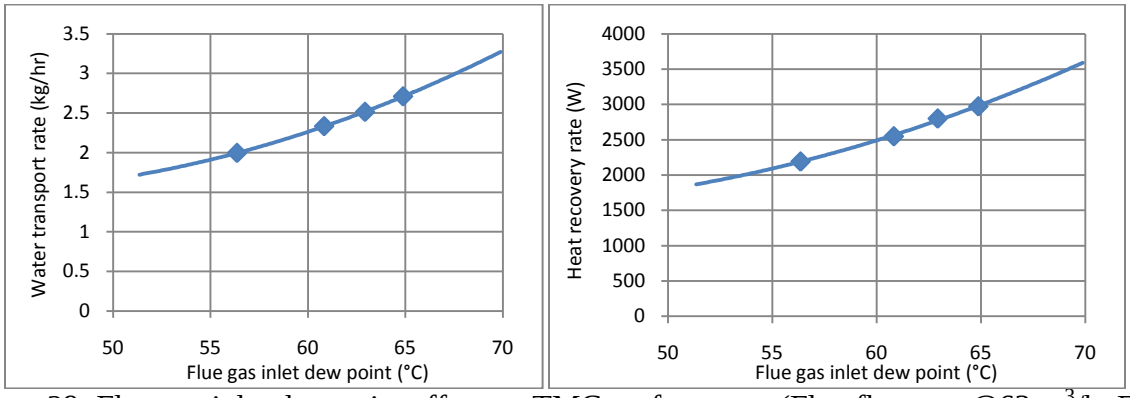

Figure 29: Flue gas inlet dew point effect on TMC performance (Flue flow rate@63 m^3/h; Flue inlet T@82°C; Water flow rate@1.25kg/min; Water inlet T@25°C)

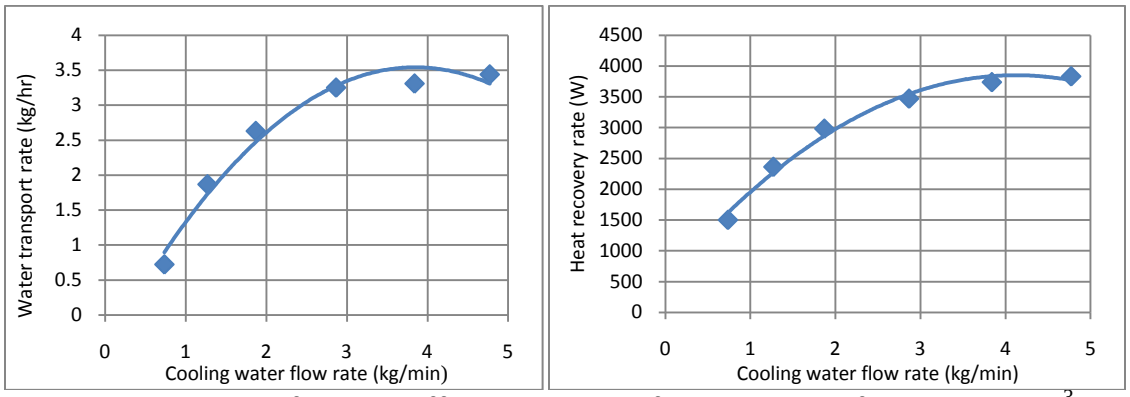

Figure 30: Cooling water flow rate effect on TMC performance (Flue flow rate@63 m^3/h; Flue inlet T@82°C; Flue inlet Td@56°C; Water inlet T@25°C)

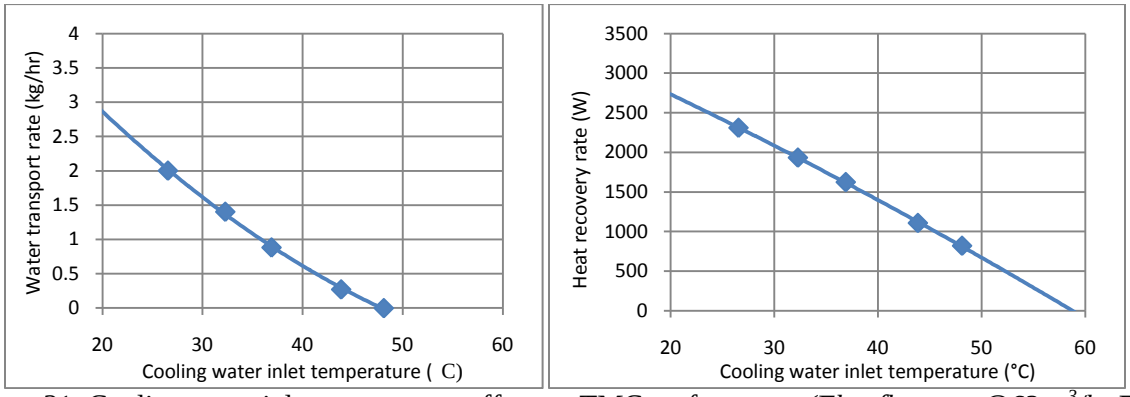

Figure 31: Cooling water inlet temperature effect on TMC performance *(Flue flow rate@63 m^3/h; Flue inlet T@82°C; Flue inlet Td@56°C; Water flow rate@1.25kg/min)*

Metallic membrane tube performance study

Besides all alumina based membrane tubes we usually used for TMC, we also developed metallic substrate based ceramic membrane tubes for this project.

Metallic membrane tubes module assembling

A 44-metallic-tube laboratory module was assembled with 38 SS434 substrate tubes and 6 SS316 substrate tubes. The tubes arrangement was as shown in Figure 32.

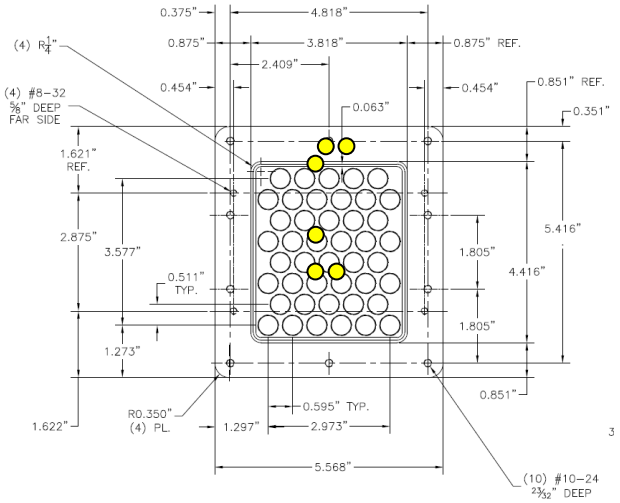

Figure 32: The stainless-steel module tube sheet drawing (yellow: SS316)

The tube sheets were made of Garolite, which has high-heat resistance, dimensional stability, and high flexural strength. The tubes are bonded to the tube sheet with Loctite E-30CL Hysol Epoxy. To minimize adhesive leak-through, we put multilayer plastic film and O-rings on both ends of the metallic tubes, and pre-glued the back surface of the tube sheets. (see Fig. 33)

Figure 33: Photos of a assembled stainless-steel substrate based membrane module

A ceramic membrane tube module with similar dimensions was built to compare the heat and water recovery performance with this metallic substrate based module. The tube outer diameter was 0.5 inch and the length was 17 inches (see Fig. 34)

Figure 34: Photo of all ceramic module (0.5-inch-OD ceramic membrane tubes)

Metallic membrane tube module water and gas transport rate measurement

Bubble testing was done to check leaks through the sealant, as well as from the end cap seal section, (see Fig.35). The highest tube inside pressure tested was 6 PSI, and there was not any leakage found.

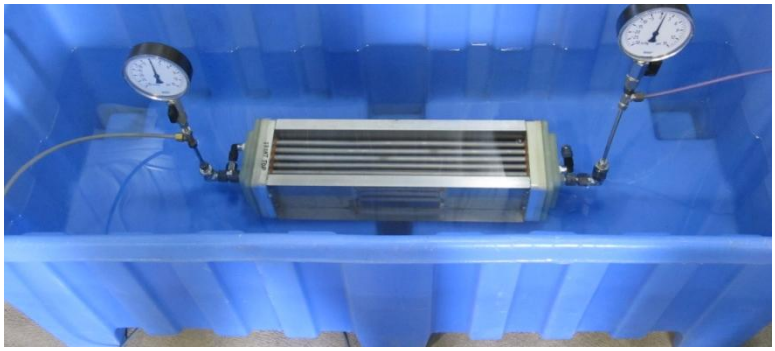

Figure 35: Metallic membrane tube module gas transport testing setup

Figure 36 shows the water transport rate testing setup, and Table 3 lists the water transport rate results at two different deionized water pressure, 3 and 6 PSI.

Figure 36: Metallic membrane tube module water transport testing setup

Metallic membrane tube module performance

Water inlet flow rates and temperatures, flue gas inlet temperatures, and water side vacuum was varied to see the metallic module performance. Figures 37 and 38 show the results. The results show higher cooling water inlet flow rate and lower cooling water inlet temperature increase the vapor condensation rate, and the metallic membrane tube module has similar performance at different vacuums. Lower inlet flue gas temperature slightly increases the condensation rate, and the highest heat recovery rate was achieved at around 170°F flue gas temperature.

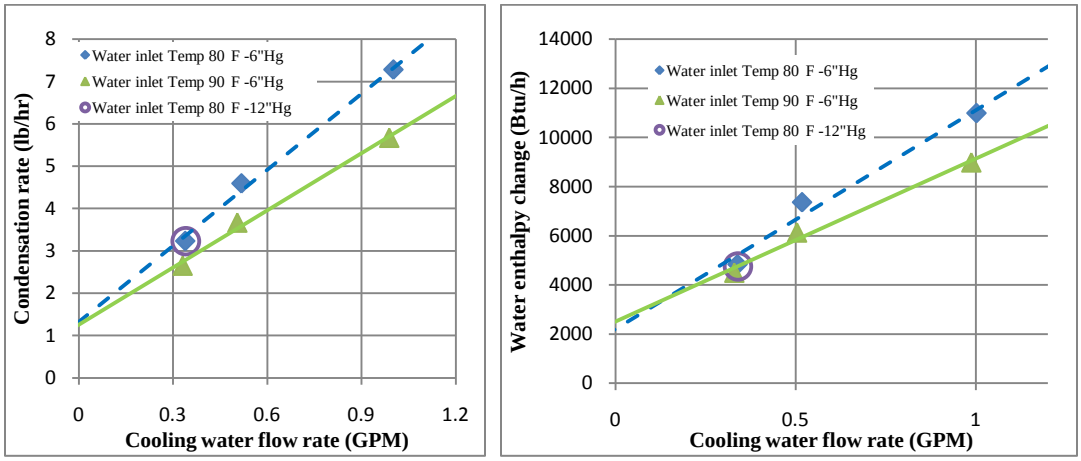

Figure 37: Cooling water flow rate, temperature, and vacuum effect on vapor condensation rate and heat recovery

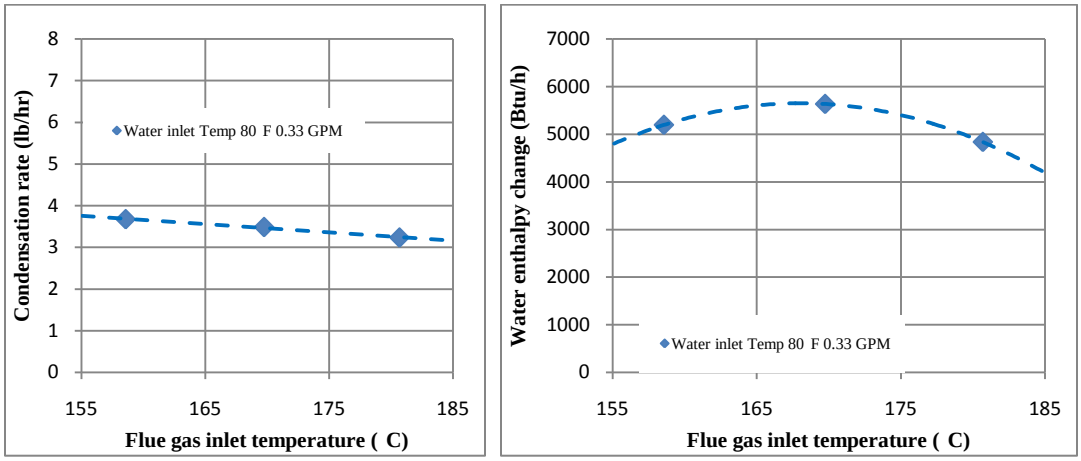

Figure 38: Flue gas inlet temperature effect on vapor condensation rate and heat recovery

We compared the module vapor condensation rate at different cooling water average temperature for three different modules (the 1st metallic membrane tube module, the 2nd metallic membrane tube module, and the all ceramic based membrane module). Dimensions for the three modules are list in Table 3, and results are shown in Fig.39. Results show similar performance for the three modules, with the ceramic tube module has a little bit higher condensation rate.

Table 3. Key parameters of the three TMC modules

	Metallic 1st	Metallic 2nd	Ceramic
Tube number	44	44	44
ID (inch)	0.410	0.40	0.335
OD (inch)	0.456	0.45	0.469
Wall thickness (inch)	0.023	0.025	0.067
Water permeate rate (lmhb)	30 to 45	30	45 to 60
Solid material thermal conductivity (W/mK)	26	26	30
Porosity	35%		20%
Effective thermal conductivity (W/mK)	17	17	24.12

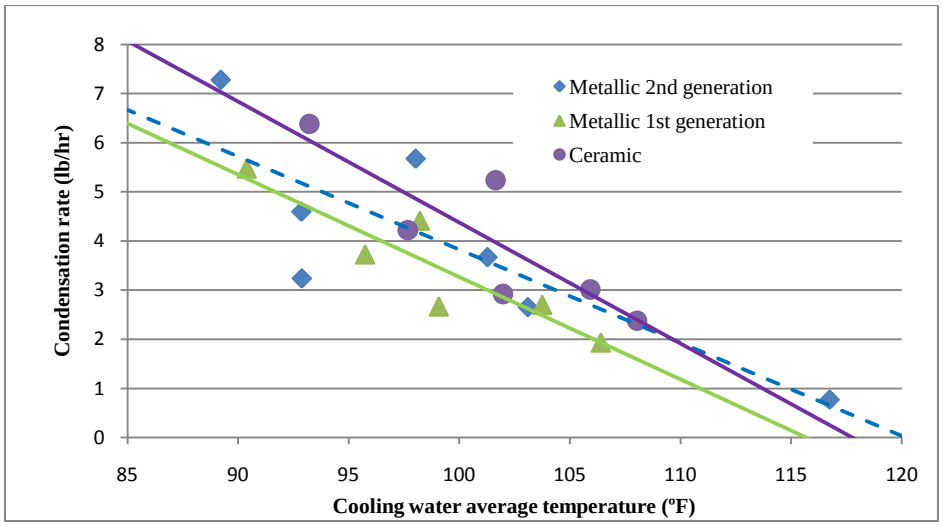

Figure 39: Three different modules vapor condensation rate comparison

SO_2 injection test

A 50 hour SO_2 injection test with hot flue gases was done to verify corrosive gas impact on the TMC module made from metallic substrate membrane tubes, and the SO_2 concentration in the

flue gas was maintained at approximately 250ppm. Figure 40 shows the photo after the test with no signs of corrosion.

Figure 40: The metallic membrane tubes module after 50-hour SO_2 injection testing

We ran similar test to measure the metallic membrane tubes module vapor condensation and heat recovery to compare the module performance before and after 50 hours SO_2 injection test, see Fig.41. The results show the vapor condensation rate are very close, and there is no significant SO_2 effect.

We measured the deionized water transport rate after SO_2 injection test and compared it with previous results. Table 4 shows there is no change for water transport rate of the metallic membrane tubes module.

Table 4. Metallic membrane tubes module water transport test results before and after 50-hours SO2 injection test

	Pressure (PSI)	Transfer rate (L/hour)	Transfer rate (lmhb)
Before SO_2 Test	3	0.296	2.17
	6	0.776	2.81
After SO_2 Test	3	0.381	2.80
	6	0.753	2.76

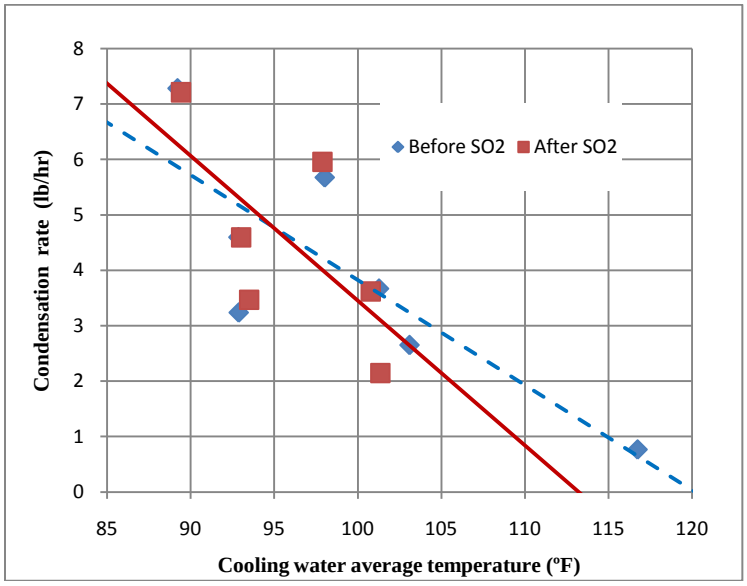

Figure 41: Comparison of module performance before and after SO_2 test

4.3 Porous metallic substrate membrane development for high transport flux

A metallic substrate membrane has many advantages over a ceramic substrate membrane, including better heat transfer performance, robustness and easy to fabricate into large modules for large industrial process use. Therefore, it is important to develop high performance metallic substrate membrane with optimum performance. Current outside membrane coating methods has

been further developed and improved to achieve higher water transport flux by using a thinner and more uniform ceramic membrane layer (an intermediate layer is not needed), eliminate membrane pin-hole defect problems, and make the tube geometry more uniform so that it can be available for future large quantity industrial module fabrication.

Tubes were formed by employing powder metallurgy technology and extruding a mixture of 15 micron 434 stainless steel powder, a binder, and a solvent through a die to form the tubular product. The tubes were sintered by first burning out the binder at 500°C in air followed by heating in 4% hydrogen in argon to 700°C before switching to flowing hydrogen for the ramp up to 1015°C followed by an hour soak at 1015°C. The furnace was cooled down to 700°C with flowing air before switching to the argon/hydrogen mixture to cool down to room temperature. The resulting support tubes had an average porosity of approximately 35% with average pore size ranging from 3.5 to 4.3 microns. The support tubes were coated on the outside surface using proprietary technology with aluminum oxide having a particle size of approximately 0.05 microns. The aluminum oxide had a high content of alpha alumina which minimizes the phase change that occurs during layer sintering. The coated tubes were sintered using the same protocol as the support tubes but with a soak temperature of 950°C.

Figure 42 shows a flow-weighted pore-size distribution representative of the membranes that were prepared for this project. Our pore-size determination system cannot accommodate samples longer than nine inches so it was not possible to evaluate the actual membranes to go into the module. All 110 membranes were evaluated for leaks by determining the bubble point in isopropanol. Out of the 110 membranes, 88 were found to have very little or no leaks with an average first bubble at 15.3 psi and full bubbling at 35.1 psi. Another 10 membranes were determined to be marginal with an average first bubble at 5.0 psi and fully bubbles at 17.8 psi. Finally, 12 membranes were found to be not acceptable. One of the cut off pieces from one of the completed membranes was mounted in epoxy and evaluated by scanning electron microscopy. Figures 43 and 44 show low and high magnification micrographs of the cross section of the tube. Figure 44 shows the layer thickness averages 4-5 microns.

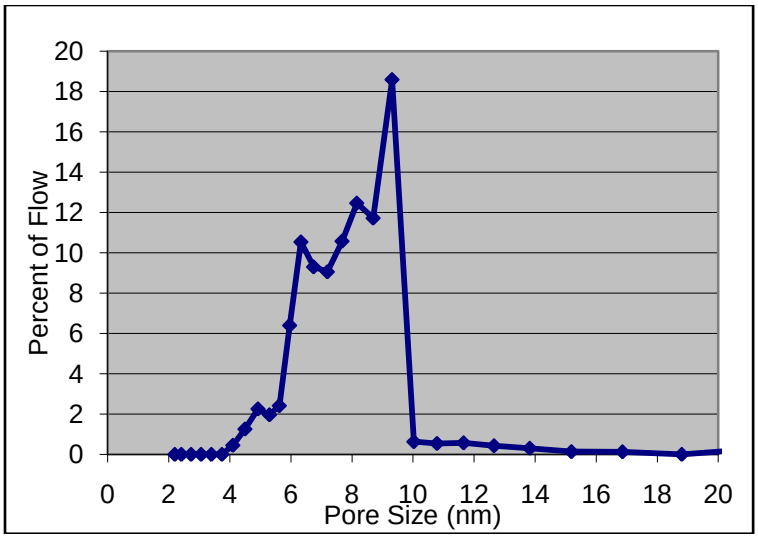

Figure 42: Typical flow-weighted pore size distribution for outside coated tubular metallic membrane

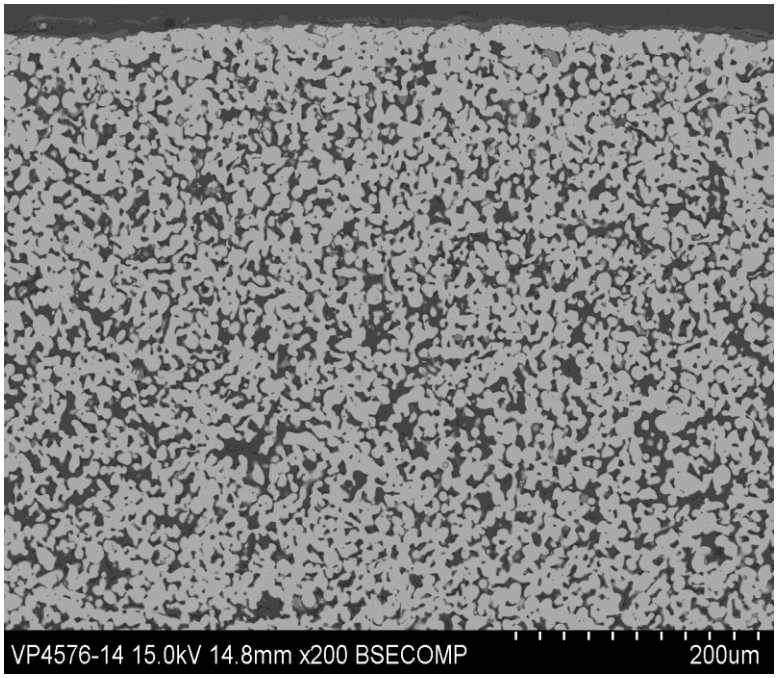

Figure 43: Scanning electron micrograph at 200X showing the alumina layer on the outside surface of the support tube.

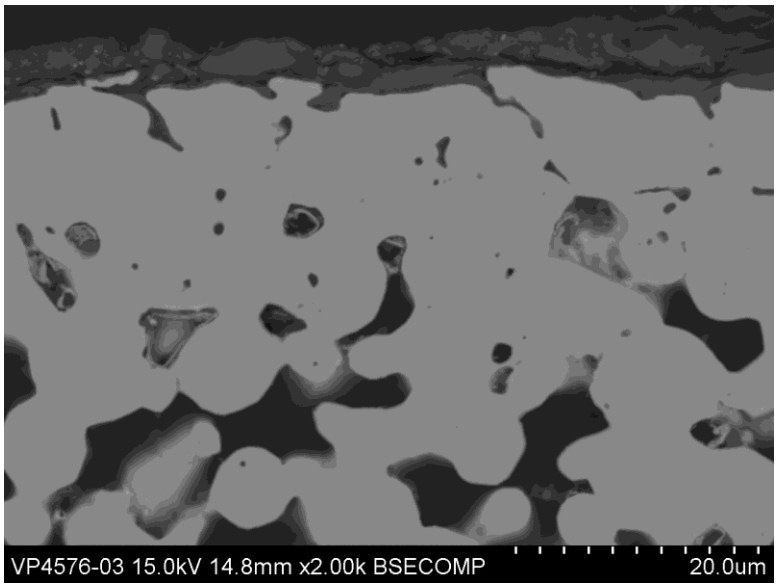

Figure 44: Scanning electron micrograph at 2000X showing an alumina layer at top of image with an average thickness of 4-5 microns.

4.4 TMC Module Design Optimization

This study focused on widely available low grade industrial waste heat applications with low temperature and high moisture contents along with significant high quality water recovery.
At high moisture content conditions, water transport flux requirement for the nanoporous membrane is much higher for removing this larger quantity of condensed water, and it is the same for heat transfer requirements where the large amounts of released latent heat needs to be removed. These depend on many factors, like membrane pore size, porosity and substrate conductivity and thickness. Therefore, different membrane pore sizes, different membrane condensing module designs have been evaluated at different simulated stream moisture content conditions, to achieve optimum energy and water recovery performance.

Besides different membrane pore sizes we have tested in the lab unit, and the metallic substrate tube development, we also worked on larger membrane module design to allow economical scale up of the TMC unit. Figure 45 shows one of the large TMC module developed, which features a 34" long membrane tube module design instead of the current 18" long module design. This can significant reduce the overall TMC unit cost. We also worked on making the TMC module part cost effective by using compression molding method, specifically for the module two end caps and two tube holder blocks (which we typically called tube sheets). The molding tool developed, can save 85% of the part costs compared with the machined parts. Pictures in Fig.46 show the original machined tube sheet in the yellow color (right side) and the compression molded tube sheet in black color (left side).

Figure 45: Longer TMC module

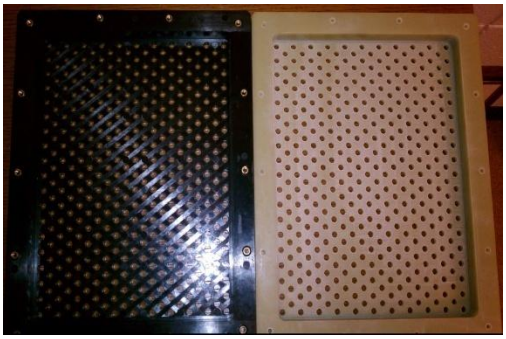

Figure 46: Tube sheet made from compression molding: (left) compared with machined part (right).

5. Benefits Assessment

TMC technology was developed for natural gas boiler flue gas heat and water recovery. The present project is giving an expansion of its use for other industrial low grade waste heat streams, many of them have much higher moisture content which is more favorable for TMC to recover more heat and water. In the process of expanding TMC applications, we found out low grade high moisture effluent is widely available from industries such as food, chemical, metal, biomass production, and etc. For example, to meet the more stringent air quality regulations, most of the effluents from these industrial processes must go through a series of cleanup procedure before being exhausted to the atmosphere. The cleanup equipment is typically a wet (or dry) scrubber, which is responsible for capturing any acid gases and particulate matters. After the scrubber, the effluent is typically in saturated condition if it is a wet scrubber, or close to saturation if a dry scrubber. This is because large amount of water is used in these kinds of scrubbers, and the effluent temperature is typically lower than 200˚F. This low temperature high moisture content effluent gas is considered low grade heat, and can not be recovered by any current available technologies. The emission of this high moisture effluent also causes environmental problem like large plume of vapor can reduce the visibility of the nearby roads, and cause local high moisture condition which can cause many problem such as corrosion of buildings and equipment. But this high moisture effluent actually has very high energy content because of the huge latent heat associated with the water vapor. Effectively recovering the water vapor and its tremendous latent heat will not only conserve energy and water, but also avoid the environmental problems.

Industrial waste heat streams identified suitable for TMC application for water recovery

High moisture effluents can be generated from many industrial processes, like food, paper and other drying processes, high hydrogen content fuel combustion processes, such as natural gas and hydrogen combustion flue gases, water quenching processes in metal making, and fermentation processes in biomass industry. Many more high moisture effluents can be generated by the post cleaning processes (different scrubbers are typically used) for many high particulate matter and high acid gas content effluents to meet air quality control criteria. For the nature of these effluents involved different industries and different processes, it is very difficult to quantify their detailed parameters and quantities. For this report we mainly focused on high moisture effluents from scrubbers, which include dry and wet scrubbers. And most often used is SO2 scrubbers, also called Flue Gas Desulfurization (FGD) units. Appendix 1 provides a detailed market evaluation of different kinds of wet scrubbers used in different industries in the US.

According to a March 2009, 13-page letter from the Austin, TX chapter of the Sierra Club to the US EPA, there are 73 different industrial processes that emit H_2S which typically need wet scrubbers to do the cleanup work. Excluding processes associated with oil and gas exploration and production, processes listed in this letter include:

- Pulp and paper mills
- Paper production
- Municipal sewage treatment plants
- Large confined animal feeding operations
- Carbon black manufacturing
- Portland cement kilns
- Municipal waste landfills
- Coke ovens
- Coal gasification plants
- Tanneries
- Slaughterhouses, chicken houses with waste incinerators, and rendering plants

- Geothermal power plants (this is a major issue in California, but there aren't any such plants in southern CA)
- Sulfur products and hydrogen sulfide production plants
- Animal fat and oil processing plants
- Asphalt storage facilities
- Blast furnaces
- Breweries and fermentation processes
- Fertilizer production
- Glue manufacturing
- Metal processing (gold ore, lead ore, lead removal, copper ore sulfidizing and metallurgy)
- Barium carbonate and barium salt production
- Phosphoric acid production
- Fish, sugar beet and sugar cane processing

Miscellaneous processes, including

- Carbon disulfide manufacture
- Dye manufacturing
- Textile printing
- Thiophene manufacturing
- Sulfur manufacturing
- Soap manufacturing
- Phosphate purification
- Hydrochloric acid purification
- Cellophane, rubber, and plastics processing
- Silk making
- Rayon making
- Pyrite burning
- Photoengraving
- Synthetic fibers manufacturing
- Polysulfide caulking manufacturing
- Bromide-bromine manufacturing
- Artificial flavors manufacturing
- Additives and sealants manufacturing
- Refrigerant chemicals manufacturing

This letter mentions that 16 states (which include major industrial states such as Texas and Ohio) have no regulations on H_2S emissions, which complicates determining the population of acid gas scrubbers. The letter mentions that the US EPA Regions that cover these 16 states have received "thousands" of complaints about H_2S odors. The letter mentions there is no accurate national emissions inventory for H_2S; the letter cites a US EPA estimate of 110 million pounds annually. Oil refineries do use acid gas scrubbers, but trying to estimate this population is speculative at best. Per the 2009 annual survey of refining capacity by Oil & Gas Journal, there are 130 oil refineries in the US (Texas: 23; Louisiana: 18; California: 15; single digit populations for the other 47 states).

Other industries that use acid gas scrubbers include

- Semiconductor manufacturing
- Food processing (kind of broad)(rendering plants)
- Asphalt manufacturing

- Metal casting (foundries)
- Chemical manufacturing, especially the production of styrene
- Surface coating operations
- Fragrance manufacturers
- Wood products

If even half of these industrial processes use acid gas scrubbers, the number in use could well be in the thousands.

TMC Potential Application for Heat and Water Recovery in Pulp and Paper Mills

According to the Center for Paper Business and Industry Studies (CPBIS), there are about 400 mills with pulp only or pulp & paper productions. Usually in pulp mills and in pulp & paper mills, wood-waste and recovery boilers as well as lime kilns are installed and operated. The exhaust streams from the boilers and kilns are rich in water vapor and have a good potential for TMC application. According to CPBIS, there are 500 to 700 other mills which are paper mills only; no pulp is produced in these mills. In these mills, pulp is supplied from other pulp or pulp & papers mills, and paper production is the main business for the mills. Usually, no wood-waste and recovery boilers and no lime kilns are in operation on paper mills.

In an integrated Pulp & Paper mill, there are several areas where TMC could be applied. Six of them are listed below.

1. Exhaust stream from paper machine ventilation system.

   -The stream is air/water vapor mixture, should be clean, temperature below 250˚F;
2. Exhaust stream from pulp dryers.

   -The stream is combustion products/water vapor mixture, should be relatively clean, temperature below 300 ˚F;
3. Wood waste firing boiler exhaust after wet scrubber or wet ESP.

   -The stream is combustion products/water vapor stream, contaminated with particulate matter (PM) and some chemicals, H_2O up to 20%, temperature below 200 ˚F;
4. Recovery boiler exhaust after cleaning units.

   -The stream is black liquor combustion products/water vapor stream, contaminated with some PM and real chemicals, H_2O up to 30%, temperature about 300+˚ F;
5. Lime kiln exhaust after wet scrubber.

   -The stream is combustion products/water vapor stream, contaminated with PM and some chemicals, H_2O up to 35%, temperature about 200 ˚F
6. Steam-stripped contaminated streams including NCG.

   -The stream contains combustibles, H_2O up to 50%, temperature below 250 ˚F.

Table 5 below provides a summary of TMC potential applications and savings, with data source cited. Residential furnace application is a new byproduct we have just developed and demonstrated last year, with two demonstrations running into the second heating season till now. In this Table, we are not able to include other acidic gas scrubbers we mentioned above, which we can not find reliable data sources.

Table 5: Summary of TMC potential applications and savings

	Energy Saving (Trillion Btu/year)	Avoided CO2 (million tons/year)
Industrial and commercial boilers*	1,207	60.4
Coal fired utility boilers with FGD**	2,535	126.8
Refining industry with wet scrubbers	18.9	0.945
Portland cement industry with wet scrubber	2.6	0.13
Iron and steel industry with wet scrubbers	5.7	0.286
Pulp and paper industry with wet scrubbers	38.5	1.924
Residential home furnaces ***	331	16.6
Total	4,139	207.1

** _"Characterization of the U.S. Industrial/Commercial Boiler Population" by Energy and Environmental Analysis, Inc. to ORNL, May 2005. Energy saving calculations are based on our demonstration experience with industrial boilers.*

***_FGD data includes both wet and semi-dry scrubbers. Energy saving calculations are based on our demonstration experience with industrial boilers. FGD is installed for about 20% of the US coal-fired utility boiler, flue gases from non-FGD units are also potential TMC users since many of the coals used are of high moisture content, but they are not counted in this report.*

****_"Residential Energy Consumption Survey", DOE Energy Information Agency, 2005. Residential home furnace energy saving calculation is based on our two home demonstrations from last year. Carbon saving calculation just bases on the energy savings.*

6. Commercialization

By working with project partners, we identified potential manufacturers and customers for this technology and developed a commercialization plan and a technology transfer strategy. TMC technology is licensed to a major boiler equipment company, for boiler flue gas application, we worked with them to commercialize the new developed technology to other waste heat and water recovery markets, and additional license agreement may be required. This company is a well known, trusted supplier of boiler heat recovery devices including economizers, vent condensers, air coolers, after coolers, and other energy efficiency devices.

- A payback period of 18 months is calculated for the current ceramic substrate based membrane tubes. Since the tube cost only accounts for 6% of the total TMC unit, currently higher cost for the metallic substrate based membrane tube will not be a show stopper for commercialization.
- While this company is now commercializing the ceramic substrate based membrane TMC to applications on boiler and beyond, they are also very interested in commercializing the metallic substrate based membrane TMC, which will provide more robustness, easy to scale up for large installation, and other features. We are working together with team partners to propose field testing the metallic membrane TMC, so this commercializer can get first-hand experience and confidence on the new material and potential new TMC module fabrication method.

7. Accomplishments

- An advanced multiphase mixture model has been developed and validated for the prediction of TMC performance and underlined transport phenomenon. Experimental study was done, and the results show condensation and convection through the porous membrane bundle was greatly improved over an impermeable tube bundle, because of the membrane capillary condensation mechanism and the continuous evacuation of the condensate film or droplets through the membrane pores.
- A detailed market study shows a broad application area for this advanced waste heat and water recovery technology. A commercialization partner has been lined up to expand this technology to this big market.
- Three papers were presented at ASME IMECE 2011:
  - ✓ D. Wang, W. Liss, and A. Bao, Water Reclamation from High Moisture Content Waste Heat Streams, IMECE2011-63513**,** ASME IMECE 2011.
  - ✓ A. Bao, D. Wang, and C.-X. Lin, Nanoporous Membrane Tube Condensing Heat Transfer Enhancement Study, IMECE2011-63530, ASME IMECE 2011.
  - ✓ C.-X. Lin, D. Wang, and A. Bo, Numerical Modeling and Simulation of Condensation Heat Transfer in a Bundle of Transport Membrane Tubes for Waste Heat and Water Recovery, IMECE2011-63756, ASME IMECE 2011.

8. Conclusions

Based on the project research activities, the following conclusions can be drawn:

- The multiphase mixture model can be used to predict water transport and phase change process in TMC walls, which is very helpful to better understand the TMC working mechanism and improve its design in the future development. Detailed flow and heat transfer data sets at different operating conditions have been produced, which provide both insight and useful information for TMC performance improvement or optimization.
- Better understanding of condensing heat transfer mechanism for porous membrane heat transfer surfaces, which shows higher condensation and heat transfer rates than solid tubes, due to existence of the porous membrane walls. Laboratory testing has documented increased TMC performance with increased exhaust gas moisture content levels, which has exponentially increased potential markets for the product. The TMC technology can uniquely enhance waste heat recovery in tandem with water vapor recovery for many other industrial processes such as drying, wet and dry scrubber exhaust gases, dewatering, and water chilling.
- Metallic substrate membrane tube development and molded TMC part fabrication method, provides an economical way for expanding this technology to larger scale applications with good payback expectation.

9. Recommendations

This research work has led to new understandings on the TMC working mechanism to improve its performance, better scale up design approaches, and economical part fabrication methods. Field evaluation work needs to be done to verify the TMC real world performance, and get acceptance from the industry, and pave the way for our commercial partner to put it into a much larger waste heat and waste water recovery market.

10. References

1. J. Boyen, Thermal Energy Recovery, JOHN WILEY & SONS, (1980).
2. Bend Research, Research on an Energy-Efficient Drying Process, DOE Final Report, DOE/ID/12293-1 (DE86013369), Feb.25, (1986).
3. H. Strathman, B. Bauer and J. Kerres, Polymer Membranes with Selective Gas and Vapor Permeation Properties, Makromol. Chem., Macromol. Symp., v. 33, p.161-178, (1990).
4. J. Randon, and R. Paterson, Preliminary Studies on the Potential for Gas Separation by Mesoporous Ceramic Oxide Membranes Surface Modified by Alkyl Phosphonic Acids, J. of membrane science, V.134, P.219-223, (1997).
5. R. Noble, S. Stern, Membrane Separations Technology Principles and Applications, Elsevier, (1995).
6. D. E. Fain; Membrane gas separation principles; MRS Bulletin/April, v.19(4); p.40-43,(1994).
7. S. Vercauteren and K. Keizer; Porous ceramic membranes: preparation, transport properties and applications; J. of Porous Materials, v.5, p.241-258, (1998).
8. M. Asaeda, L. Du and K Ikeda: Experimental studies of dehumidification of air by an improved ceramic membrane; J. of Chemical Engineering of Japan, v.3, p.238-240, (1986).
9. J. Falconer, R. Noble and D. Sperry, Catalytic membrane reactors, In: R. Noble and S. Stern (Eds.), Membrane Separations Technology, Elsevier, Amsterdam, (1994).
10. M. Qiu and S. Hwang, Continuous Vapor-Gas Separation with a Porous Membrane Permeation System, J. Membrane Science, v. 59, p. 53-72, (1991).
11. R. Uhlhorn, K. Keizer, and A. Burggraaf, Gas Transport and Separation with Ceramic Membranes. Part I Multilayer Diffusion and Capillary Condensation, J. Membrane Science, v. 66, p. 259-269, (1992).

11. Appendices

Appendix 1: Wet Scrubber and High Moisture Exhaust Gas Market for Transport Membrane Condenser Technology